Journal of Alloys and Compounds 379 (2004) 95–98

Journal of ALLOYS AND COMPOUNDS

www.elsevier.com/locate/jallcom

# The phase diagram of the system LiF–$GdF_3$

I.M. Ranieri [a,*], A.H.A. Bressiani [b], S.P. Morato [a], S.L. Baldochi [a]

[a] *Center for Lasers and Applications, Inst. Pesquisas Energeticas & Nucl., CP 11049, Butantã 05422-970, São Paulo, SP, Brazil*
[b] *Center for Material Science and Technology, IPEN, CP 11049, Butantã 05422-970, São Paulo, SP, Brazil*

Received 15 December 2003; received in revised form 10 February 2004; accepted 10 February 2004

**Abstract**

The phase diagram of the system LiF–$GdF_3$ has been revised, using differential thermal analysis (DTA). We observed a eutectic reaction at 25 mol% of $GdF_3$ and 698 °C and a peritectic reaction at 34 mol% of $GdF_3$ and 755 °C. We found indications for a $GdF_3$ phase transformation from hexagonal to orthorhombic at 900 °C. An identification of the formed phases was made by X-ray diffraction and SEM.


*Keywords:* Phase equilibrium; Binary systems; Rare earth fluorides; DTA

## 1. Introduction

The phase diagram of the system LiF–$GdF_3$ was studied by Thoma et al. in 1960s [1,2], and it was found that it presents two invariant points: a eutectic at 26 mol% $GdF_3$ and 700 °C, a peritectic at 39 mol% $GdF_3$ and 755 °C and a $GdF_3$ phase transformation from hexagonal to orthorhombic at 875 °C. $LiGdF_4$ is the only intermediary compound, showing an incongruent melting behavior. Pham et al. [3] revised superficially this diagram determining the following values: a eutectic at 20 mol% $GdF_3$ and 627 °C and a peritectic at 32 mol% $GdF_3$ and 727 °C.

$LiGdF_4$ crystals are suitable for doping with light rare earth ions with a particular interest in neodymium ions to develop new laser media [4,5]. To grow good quality crystals from the melt the knowledge of the peritectic composition is important in order to minimize the excess of one of the components, because this excess acts as impurity causing defects (as inclusions) in the crystals. For this reason we aimed at examining this diagram more carefully, using differential thermal analysis (DTA) to construct the phase diagram. The formed phases have been identified by X-ray diffraction and the microstructure of some samples has been examined using scanning electron microscopy.

## 2. Experimental procedures

The samples utilized to construct the LiF–$GdF_3$ phase diagrams were prepared from LiF (99.9%, Aldrich), previously purified by zone refining under a flux of hydrofluoric acid (HF) and argon (Ar) gases. $GdF_3$ was obtained by $Gd_2O_3$ (99.99%, Alfa Aesar) hydrofluorination at high temperature in HF atmosphere. Samples weighting around 5 g with different compositions were melted in the same atmosphere and then pulverized for homogenization.

DTA curves were obtained in a TGA–DTA equipment, model 2960, TA Instruments. The samples weighing around 50 mg were placed in open platinum crucibles without a reference material. The measurements were performed under a flux of purified helium, with a heating rate of 10 °C/min. These conditions allowed that the broad melting curves could be resolved. The measurements were performed for temperatures up to 900 °C, because above this temperature there was a sensible loss of mass causing data scattering under these conditions the maximum loss of mass was about 1%.

The reasons for this mass loss are the evaporation of LiF and the high reactivity of the rare earth fluorides with residual air or moisture present during the experiment at high temperatures [6]. The evidence of some contamination was confirmed during the determination of the rare earth fluoride melting points, they could be obtained only with heating rates of 40 °C/min; otherwise, the samples were completely converted into the oxide above 900 °C. Therefore, for the

* Corresponding author. Tel.: +55-11-3816-9306; fax: +55-11-3816-9315.
*E-mail address:* iranieri@net.ipen.br (I.M. Ranieri).

0925-8388/$ – see front matter © 2004 Elsevier B.V. All rights reserved.
doi:10.1016/j.jallcom.2004.02.010

construction of the phase diagram we considered only the range of compositions up to 60 mol% $GdF_3$, this limit being set by the peak temperatures of the transformations in the heating mode. Sealed crucibles or evacuation of the system prior the measurements would minimize this effect.

To determine the phases present in each of the two-phase region of the phase diagrams, two samples of each composition were melted under a flux of hydrogen fluoride gas and cooled at a rate of 15 °C. One of the samples was examined using a scanning electron microscope model XL30, from Philips, and the phase compositions were estimated with an energy-dispersive spectrometer model EDXAUTO, from EDAX. The other sample was pulverized for analysis by powder X-ray diffraction, using a Bruker AXS diffractometer, model D8 Advance, operated at 40 kV and 30 mA, in the $2\theta$ range of 18–66°. The lattice constants of the identified phases were obtained by least squares fittings.

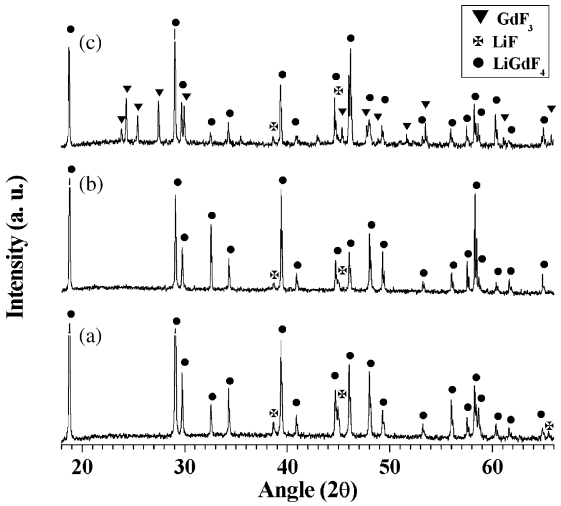


Fig. 2. X-ray curves of the samples: (a) 76 mol% LiF:24 mol% $GdF_3$, (b) 68 mol% LiF:32 mol% $GdF_3$, (c) 50 mol% LiF:50 mol% $GdF_3$.

## 3. Results and discussion

In Fig. 1, we present the phase diagram obtained for the LiF–$GdF_3$ system. We found a eutectic reaction at 25 mol% of $GdF_3$ and 698 °C and a peritectic reaction at 34 mol% of $GdF_3$ and 755 °C. The eutectic composition is in agreement with that obtained by Thoma et al. [2], while the peritectic composition agrees with that obtained by Pham et al. [3]. The reaction temperatures are in accordance with those observed by Thoma et al. despite the measurements were done during cooling of the samples. These authors used a method specified as a fast cooling with higher cooling rates than that used in conventional DTA equipments. It can then be concluded that the samples were not supercooled.

The identification of the phases present in each two phases region was performed by X-ray diffraction for the following compositions: (a) 76 mol% LiF:24 mol% $GdF_3$ (Gd24), (b) 68 mol% LiF:32 mol% $GdF_3$ (Gd32), and (c) 50 mol% LiF:50 mol% $GdF_3$ (Gd50). The X-ray curves of these samples shown in Fig. 2 confirm that the LiF and $LiGdF_4$ phases

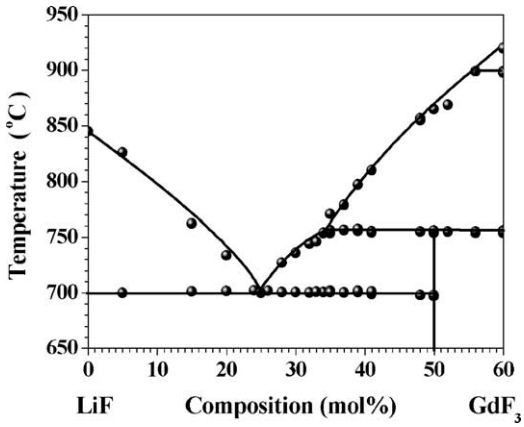


Fig. 1. The phase diagram determined for the LiF–$GdF_3$ system.

are present in the samples Gd24 and Gd32 (Fig. 2a and b), and LiF, $LiGdF_4$, and $GdF_3$ in sample Gd50 (Fig. 2c).

The lattice parameters of $LiGdF_4$ and $GdF_3$ obtained by XRD are presented in Table 1. They are in accordance with those cited in the literature [7,8].

The microstructures were observed by SEM and the phases present were identified also by EDS for the following samples: (a) 76 mol% LiF:24 mol% $GdF_3$ (Gd24), (b) 74 mol% LiF:26 mol% $GdF_3$ (Gd26), (c) 68 mol% LiF:32 mol% $GdF_3$ (Gd32), and (d) 50 mol% LiF: 50 mol%$GdF_3$ (Gd50).

The sample Gd24 presented a microstructure (Fig. 3) formed by LiF dendrites (dark regions) and a fine structured eutectic formed by LiF/$LiGdF_4$ mixture (lighter regions). In Fig. 3, the LiF primary phase is present in many locations of the analyzed area but the eutectic microstructure is dominant. It can be seen that during the solidification various crystallization fronts occurred simultaneously, generating a colony structure. The eutectic microstructure changes from a disordered arrangement of the LiF/$LiGdF_4$ phases near the LiF dendrites to a regular one with a fine fibrous morphology. Therefore, the sample composition was very close to the eutectic composition, though hypoeutectic in character.

The microstructures of the sample G26 consist almost entirely of eutectic colonies with the same fibrous morphology (Fig. 4a) and in a small area crystallization of the $LiGdF_4$ primary phase took place (gray part of Fig. 4b). This is due to the sample composition being slightly richer in $GdF_3$ than the eutectic composition. In fact, considering the eutectic composition determined in the phase diagram (Fig. 1), one expects the solidification of 4% of the $LiGdF_4$, thus, confirming that the eutectic composition is around 25 mol% $GdF_3$.

The intermediary composition of the sample Gd32, between the eutectic and peritectic invariant points, exhibited the $LiGdF_4$ primary phase. This phase was formed on

Table 1
Values obtained for the lattice parameters of the phases present in the LiF–$GdF_3$ system

| Lattice parameters | Composition $(1-x)$LiF–$x$$GdF_3$ (mol%) | | | | | |
|---|---|---|---|---|---|---|
| | $LiGdF_4$ ($x = 24$) | $LiGdF_4$ ($x = 32$) | $LiGdF_4$ ($x = 50$) | $LiGdF_4$ [7] | $GdF_3$ ($x = 50$) | $GdF_3$ [8] |
| $a$ (Å) | 5.222 (1) | 5.223 (1) | 5.225 (1) | 5.219 | 6.571 (3) | 6.570 |
| $b$ (Å) | | | | | 6.995 (4) | 6.984 |
| $c$ (Å) | 10.985 (4) | 10.986 (1) | 10.987 (3) | 10.97 | 4.393 (2) | 4.393 |
| Volume (Å$^3$) | 299.56 (21) | 299.67(70) | 299.95 (16) | | 201.92 (28) | 201.63 |

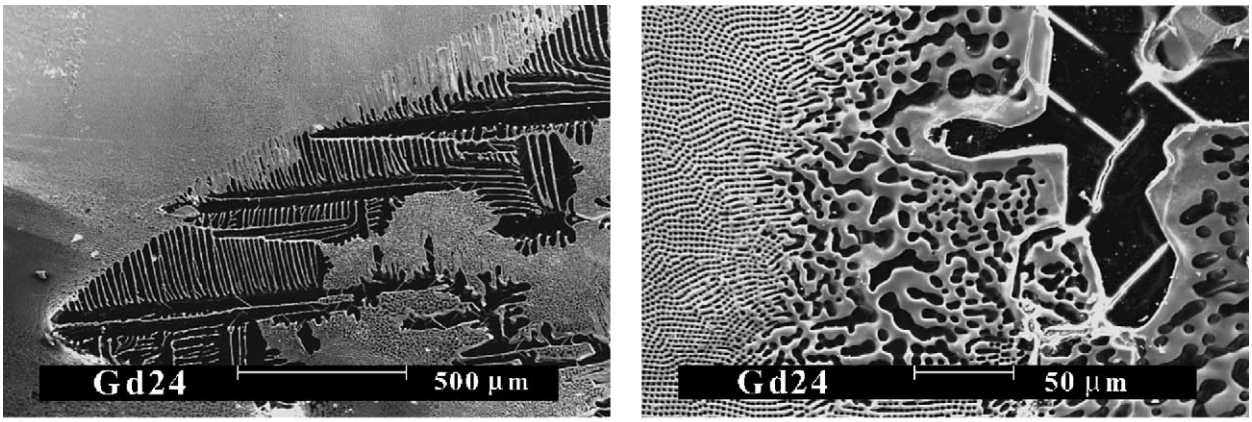


Fig. 3. Gd24 SEM photographs, in two different regions of the sample: (a) dendrites of the primary phase (dark region), (b) region where the eutectic is dominant (light gray regions).

the bottom of the ingot that was in contact with the Pt crucible and the first one to solidify. In Fig. 5, one can see that the fibrous eutectic colonies surround the primary phase.

Finally the solidification of the $LiGdF_4$ stoichiometric composition begins with the crystallization of the $GdF_3$ primary phase (gray regions in Fig. 6). When the sample temperature reaches the peritectic temperature, formation of the stoichiometric phase takes place (dark gray regions) ensuing from the reaction of the primary phase with the liquid. As the peritectic reaction is time-consuming, the $LiGdF_4$ phase is formed only on the $GdF_3$ grain boundary. In consequence of the high cooling rate there was not enough time for dissolution of the primary phase generating a non-equilibrium condition and then the simultaneous crystallization of the eutectic mixture $LiGdF_4$/LiF.

This high incongruent melting behavior of $LiGdF_4$ makes the crystal growth from the melt difficult, as observed by Ranieri et al. [9], when the peritectic composition was utilized. The crystals were very sensitive to variations in di-

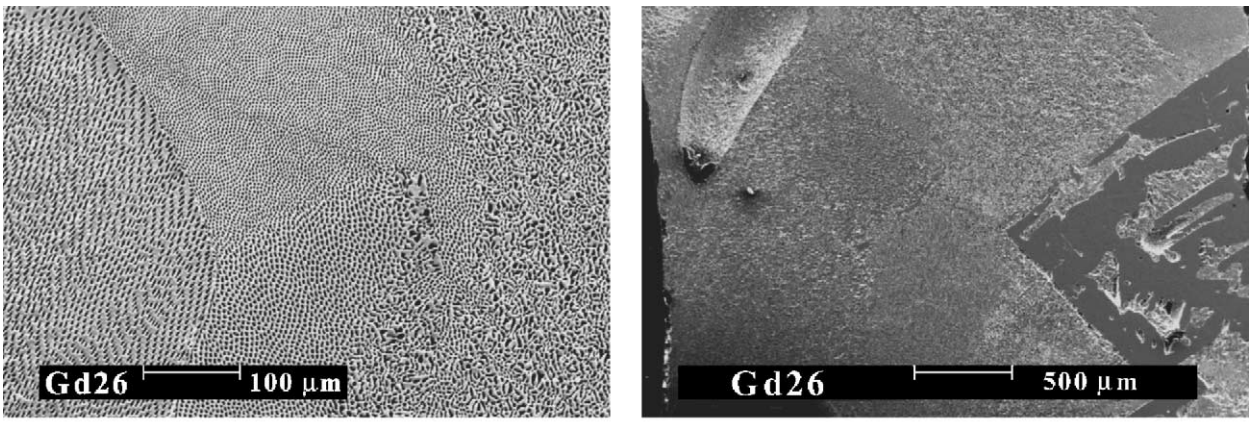


Fig. 4. Gd26 SEM photographs, in two different regions of the sample: (a) dominant fibrous eutectic microstructure (light gray regions), (b) $LiGdF_4$ primary phase (gray region).

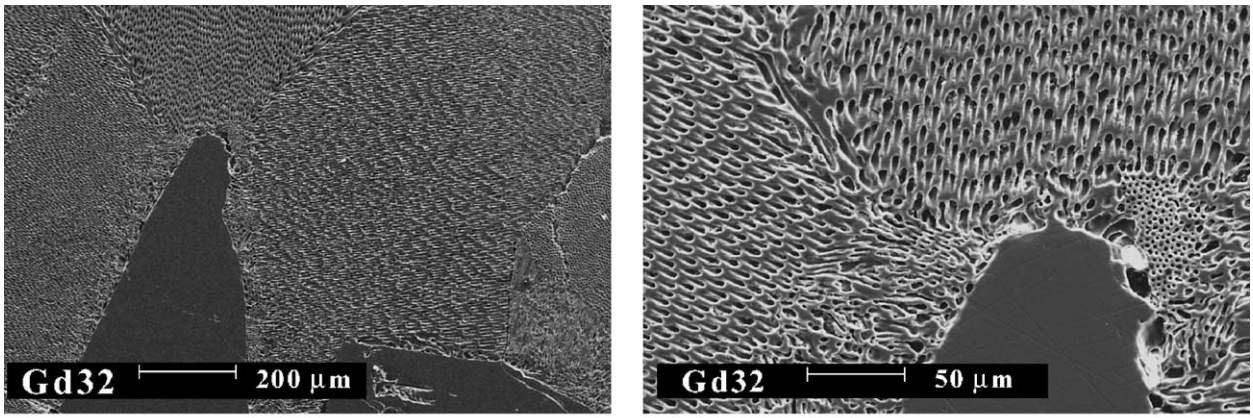


Fig. 5. Gd32 SEM photographs: (a) $LiGdF_4$ primary phase (dark gray region), (b) detail of the eutectic microstructure (light gray region).

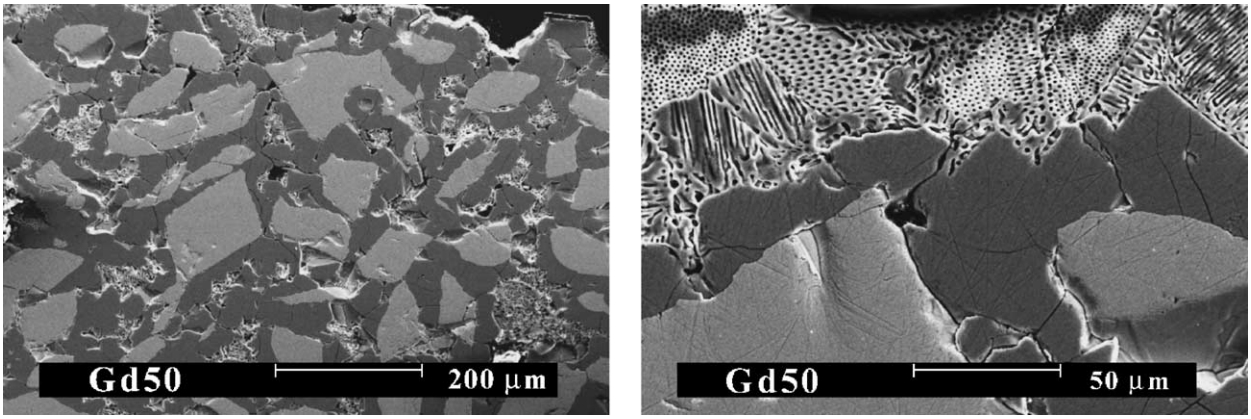


Fig. 6. Gd50 SEM photographs, in two different regions of the sample with the $LiGdF_4$ (dark gray regions), $GdF_3$ (gray regions), and the eutectic (light gray regions).

ameter and presented inclusions, also using raw materials with high purity and a reactive $CF_4$ atmosphere. The liquid presented high viscosity, which interferes in the convective flow of the melt and inhibits mixing of the melting components.

## 4. Conclusions

An accurate phase diagram of the system LiF–$GdF_3$ was determined, showing that this system presents a eutectic at 25 mol% $GdF_3$ and 700 °C and peritectic at 34 mol% $GdF_3$ and 753 °C. The diagram obtained in this work shows that the range of compositions in which one can grow $LiGdF_4$ crystals is narrower than that expected initially, limiting the amount of mass to be extracted during the crystal growth process.

## References

[1] R.E. Thoma, in: L. Eyring (Ed.), Progress in the Science and Technology of the Rare Earths, vol. 2, Pergamon Press, Oxford, 1966, pp. 90–122.
[2] R.E. Thoma, G.D. Brunton, R.A. Penneman, T.K. Keenan, Inorg. Chem. 9 (1970) 1096.
[3] A. Pham, J. Lefaucheur, G. Lutts, B. Chai, J. Nicholls, in: A.A. Pinto, T.Y. Fan (Eds.), OSA Proceedings on Advanced Solid State Lasers, vol. 15, Optical Society of America, Washington, DC, 1993, pp. 178–184.
[4] X.X. Zhang, M. Bass, A.B. Villaverde, J. Lefaucheur, A. Pham, B.H.T. Chai, Appl. Phys. Lett. 62 (11) (1993) 1197–1199.
[5] L.C. Courrol, E.P. Maldonado, L. Gomes, N.D.I.M. Ranieri, S.P. Morato, N.D. Vieira Jr., Opt. Mater. 14 (2000) 81–90.
[6] R.C. Pastor, M. Robinson, Mater. Res. Bull. 9 (1974) 569–578.
[7] G. Keller, H. Schmutz, J. Inorg. Chem. 27 (1965) 900–901.
[8] A. Zalkin, D.H. Templeton, J. Am. Soc. 75 (1953) 2453–2458.
[9] I.M. Ranieri, K. Shimamura, K. Nakano, T. Fujita, L.C. Courrol, S.P. Morato, T. Fukuda, J. Crystal Growth 217 (1–2) (2000) 145–150.